


RESEARCH LETTER

Open Access



Changes in nutrient stoichiometry in responding to diatom growth in cyclonic eddies

Kuanbo Zhou^{1†}, Yanping Xu^{1†}, Shuh-Ji Kao¹, Peng Xiu², Xianhui Wan³, Bangqin Huang⁶, Xin Liu⁶, Chuanjun Du⁵, Jun Sun⁴, Zhenyu Sun¹ and Minhan Dai^{1*} 

Abstract

Nutrient stoichiometry (e.g., nitrate + nitrite to soluble reactive phosphorus, refer to N + N/SRP, N/P hereafter) governs growth, competition and niche partitioning of phytoplankton in the illuminated oceans. The N/P, however, varies widely across the ocean and the underlying mechanisms remain unclear. Here, we report direct observations of significant variations in N/P in response to different life stages of two cyclonic eddies observed in the western South China Sea. High N/P (19.1 ± 6.9) values were observed around the nitracline in a mature-stage eddy, whereas a decay-stage eddy was characterized with low N/P (14.4 ± 4.1). The elevated N/P ratios accompanied by enriched fucoxanthin (pigment for diatom) and biogenic silica around the nitracline suggest that eddy pumping enhanced the growth of diatom which preferentially uptakes P relative to N in the mature stage of the eddy. Such high N/P ratios in the upper ocean could be reproduced if diatom uptake ratio was set between 10 and 16 in a data constrained numerical model. The preferential P uptake by enhanced diatom growth might reduce the P supply to the surface ocean, which is critical for N_2 -fixers. The transient changes in nutrient stoichiometry associated within the life cycle of cyclonic eddies also challenges the parameterization of physical–biogeochemical models with fixed phytoplankton uptake stoichiometry ratios, which could lead to bias of the model output for phytoplankton dynamics in oligotrophic ocean, where eddies frequently occur.

Keywords Non-Redfield nutrient ratio, Cyclonic eddy, Diatom, Nitrogen fixation, Western South China Sea

Introduction

The constant elemental stoichiometry of phytoplankton (C:N:Si:P = 106:16:16:1) is known as the Redfield ratio. It is considered as a foundation of ocean biogeochemistry, and also reflects the utilization of dissolved nutrients by marine phytoplankton (Falkowski 2000; Redfield 1958). Growing evidence show, however, that dissolved nutrient ratios vary widely in different oceanographic settings (e.g., Deutsch and Weber 2012). Along with the availability of nitrogen (N) and phosphorus (P), as well as other nutrients, such as silicon (Si) and iron, the nutrient ratios largely determine the phytoplankton community structure in the ocean (Deutsch and Weber 2012).

Non-Redfield ratios have been observed in various oceanic settings: coastal upwelling systems (Bruland et al.

[†]Kuanbo Zhou and Yanping Xu contribute equally to this work.

*Correspondence:
Minhan Dai
mdai@xmu.edu.cn

¹ State Key Lab of Marine Environmental Science & College of Ocean and Earth Sciences, Xiamen University, Xiamen 361102, China

² State Key Laboratory of Tropical Oceanography, South China Sea Institute of Oceanology, Guangzhou 510301, China

³ Department of Geosciences, Princeton University, Princeton NJ08544, USA

⁴ College of Marine Science and Technology, China University of Geosciences (Wuhan), Wuhan 430074, China

⁵ State Key Laboratory of Marine Resource Utilization in South China Sea, Hainan University, Haikou 570228, China

⁶ State Key Laboratory of Marine Environmental Science & College of Environment and Ecology, Xiamen University, Xiamen 361102, China

2005; Hutchins and Bruland 1998), mesoscale eddies (Li and Hansell 2008), micro-mesocosm and iron fertilization sites (DeBaar et al. 1997). The underlying mechanism for such variation, however, remains debatable and/or uncertain. Martiny et al. (2013) demonstrated a global pattern of N/P ratios in particulate form in the oceans, of which elevated ratios were observed in nutrient depleted subtropical gyres (e.g., particulate N/P = 37) and reduced ratios were found in nutrient enriched, high latitude regions (e.g., particulate N/P = 11). Such variable particulate stoichiometry is mainly driven by the variable uptake ratio and/or growth rate among different dominant phytoplankton groups for resource competition (Klausmeier et al. 2004). For example, picoplankton tends to dominate in oligotrophic regions and assimilate nutrients with a higher N/P ratio (relative to the Redfield ratio of 16), while large diatom cells are dominant in high nutrient regions with a lower N/P uptake ratio (Arrigo et al. 1999; DeVries 2018). On the other hand, high dissolved N/P ratios were observed in the subsurface of BATS station (Bermuda Atlantic Time-series Study, 31°40'N, 64°10'W) and the cause for such high N/P ratios was attributed to N addition from remineralization of N₂-fixation (Deutsch and Webber 2012). Overall, nutrient stoichiometry and the composition of the phytoplankton assemblage show reciprocal causation in the illuminated ocean.

The ubiquitous existence of mesoscale eddies may further complicate the nutrient dynamics in the oligotrophic oceans (Benitez-Nelson and McGillicuddy 2008). In the subtropical ocean, new nutrients could be brought up into the sunlit zone by eddies to change the community composition and fuel the growth of phytoplankton (McGillicuddy 2016; Xiu and Chai 2020), and thus potentially alter the nutrient stoichiometry. It was estimated that nutrient influx induced by eddies could account for ~50% of new production in the subtropical ocean (McGillicuddy et al. 1998). The activity of eddies may potentially trigger the growth of large diatoms and shift the nutrient ratios within these eddies (Benitez-Nelson et al. 2007; Li and Hansell 2008); the duration of such diatom blooms is transient and largely determined by the temporal evolution of eddy dynamics (Sweeney et al. 2003; Rii et al. 2008; Zhou et al. 2020). We hypothesize that nutrient ratios change at different developmental stages of eddies according to the succession of phytoplankton community.

Using a stoichiometrically explicit model of phytoplankton physiology and resource competition, Klausmeier et al. (2004) demonstrated a wide range of the optimal N/P ratio for phytoplankton depending on the ecological conditions, and they also suggest focusing on the variability of the nutrient ratios with high temporal and spatial resolution rather than adapting the averages.

However, no consecutive field measurements have been made in oligotrophic ocean to clearly link the transition of nutrient stoichiometry to phytoplankton succession driven by mesoscale eddies.

In this study, high spatial resolution (0.5 degree) sampling was carried out in two cyclonic eddies (CEs) in different stages of evolution in the western South China Sea (SCS). Nutrients (including ratios) and the phytoplankton community were measured to examine their interaction and determine whether non-Redfield ratios occurred within eddy systems. In parallel, particulate organic carbon (POC), particulate nitrogen (PN), and biogenic silica (bSiO₂) were measured to evaluate how the shift in nutrient ratios was reflected in the particulate phase. In addition, an ecosystem model was used to simulate and verify the nutrient uptake ratios in the eddy (Additional file 1).

Materials and methods

Sample collection

The sampling information for the two eddies has been detailed in the companion study of Zhou et al. (2020). Briefly, discrete water samples were collected with 10 L Niskin bottles guided by a Seabird SBE 911 conductivity–temperature–depth (CTD) sensor. Samples for nitrite (NO₂⁻), nitrite + nitrate (NO₂⁻ + NO₃⁻, N+N hereafter), SRP, and silicic acid (Si(OH)₄), were collected in the upper 300 m. The depth interval is set as 0, 25, 50, 75, 100, 150, 200, 250, 300 m and the depth of subsurface chlorophyll maximum (SCM). Water samples for analysis of particulate matter (POC, PN, and bSiO₂) and concentration of the diatom diagnostic pigment (i.e., fucoxanthin) were collected in the upper 150 m (i.e., 0, 25, 50, 75, 100, 150 m). Sampling methods have been detailed in Zhou et al. (2020).

Nutrient analysis

Macronutrients were measured by a semi-automatic flow injection nutrient analyzer Tri-223 (Pai et al. 1990a, 1990b). We used the deep-sea water (DSRMNS) collected from ~3000 m in the South China Sea basin with validated concentrations as the reference material during the cruise. The analytical precision was ±1.5% ([NO₂⁻] = 0.8 μmol L⁻¹), ±4.2% ([SRP] = 1.6 μmol L⁻¹) and ±2% ([Si(OH)₄] = 10 μmol L⁻¹), respectively, during the cruise. The relative error between DSRMNS and RMNS (produced by KANSO TECHNOS CO., LTD (http://www.kanso.co.jp/eng/production/available_lots.html)) was controlled below 2% in our nutrient lab. The precisions were estimated as the standard deviations of repeated measurements (>10 times) of the reference solutions. The analytical precisions are included for the ratio calculation through error propagations. In addition, the low SRP concentrations (<500 nmol L⁻¹), analysis

was carried out using a home-made, ship-board C18 enrichment-flow injection analysis system (See details in Ma et al. (2008)). The analytical precision of this method was $\pm 8\%$ (10–200 nmol L⁻¹) and $\pm 5\%$ (200–500 nmol L⁻¹). Nutrient samples were analyzed immediately onboard after sampling or refrigerated at 4 °C and analyzed within 3–6 h of sampling (Xu et al. 2009).

Biogenic silica, pigment, POC and PN analysis

POC, bSiO₂ and pigment data have been presented in Zhou et al. (2020). Here, we include Particulate N data for the calculation of elemental ratios in particulate form. It was determined using a PerkinElmer®-2400 Series II CHNS/O elemental analyzer (USA) (Zhou et al. 2013). The procedural nitrogen blank was $<0.06 \mu\text{mol N L}^{-1}$, and the uncertainty for the PN data was $<10\%$. The fluorescence data were obtained from a Wetlabs fluorometer interfaced with the CTD. The fluorometer had been calibrated by measured Chl *a* from the discrete samples.

Model experiment setup

A data-constrained model was developed and used to examine the dynamics between the phytoplankton non-Redfield uptake ratio and the nutrient stoichiometry in the eddy cores. A two-step approach was employed. The eddy nutrient distributions that were driven purely by upwelling were rebuilt using measured nutrient profiles in the non-eddy region and vertical velocities calculated from the quasi-geostrophic Omega equation in the eddy core (Hu et al. 2011; Zhou et al. 2020). These derived nutrients profiles were then used to initialize and drive the biogeochemical Carbon, Silicate, Nitrogen Ecosystem (CoSiNE) model (see equations and parameters in Ma et al. 2019). During the modelling process, measured phytoplankton concentrations were applied in the model and kept unchanged during a 2-week period. Runs with different phytoplankton uptake ratios were conducted to investigate how these might affect nutrients' distributions. To examine the role of diatoms on the variability of nutrient ratios, the uptake ratio by non-diatoms was set as the Redfield ratio and that for diatoms was fine-tuned until the model-derived nutrient ratios best fit the observed ones.

Results

Three-dimensional nutrient structure of the cyclonic eddies

Detailed physical and biogeochemical features of the two CEs were described in Zhou et al. (2020) and Hu et al. (2011). Briefly, C1 was measured during its decay stage (decay eddy hereafter) at 47–55 days of age, as elucidated by the temporal evolution of the Sea Level Anomaly (SLA) (Zhou et al. 2020). As shown in Fig. 1,

the center of decay eddy was located at 112 °E, 14°N. The C2 eddy (centered at 111 °E, 11.5 °N) was observed to the south of decay eddy with a similar core diameter of 60–90 km. C2 was sampled during its mature stage at an age of 15–20 days (mature eddy hereafter). The hydrography indicated that the upward water displacement was more pronounced in mature eddy than decay eddy. The upwelling rate at the center of mature eddy was 4.0 m d⁻¹ and that is only 0.7 m d⁻¹ for decay eddy (Zhou et al. 2020).

As shown in Figs. 1 and 2, N+N, SRP and Si(OH)₄ concentrations all demonstrated upward doming as a result of eddy pumping. Their distributions presented an irregular “circular cone-like” shape within the eddies. The eddy-influenced area of enhanced nutrient levels is usually smaller at the surface, but larger at the subsurface. Clearly, nutrient concentrations were elevated in eddy cores relative to their surrounding waters at the same depth (Fig. 2).

Nutrient depth profiles showed substantial vertical displacement across the eddy core section (Fig. 2). Nutrient-enriched subsurface water with concentrations of 13.3 $\mu\text{mol L}^{-1}$ N+N, 0.86 $\mu\text{mol L}^{-1}$ SRP, and 12.8 $\mu\text{mol L}^{-1}$ Si(OH)₄ in decay eddy rose to ~70–80 m along the specific density, $\sigma_{\theta}=25$ isopycnal surface from ~150 m (the depth where a similar nutrient level was observed outside the eddy). Such water displacement was even more pronounced in mature eddy, where nutrient-enriched subsurface water concentrations of 16.3 $\mu\text{mol L}^{-1}$ N+N, 1.08 $\mu\text{mol L}^{-1}$ SRP, and 16.4 $\mu\text{mol L}^{-1}$ Si(OH)₄ could be brought from ~160 m up to 50 m along the $\sigma_{\theta}=25$ isopycnal surface. The difference in upward water displacement between the two eddies also affected the nutrient inventory of 0–100 m depth interval (Table 1).

For both eddies, the depth of the upper nutriclines coincided with the depth of SCM. The average of depth integrated nutrient concentration (0–100 m) in mature eddy was significantly elevated relative to non-eddy references ($P < 0.05$, *t* test). In detail, N+N, SRP and Si(OH)₄ concentration was, respectively, 378%, 338% and 209% of those in non-eddy references. Similarly, the nutrient concentrations in decay eddy were higher than the references ($P < 0.05$, *t* test), but with a less degree as compared to mature eddy. The N+N, SRP and Si(OH)₄ concentration was 290%, 269% and 183% of non-eddy references, respectively. Compared to N+N and SRP, the difference of Si(OH)₄ concentrations between two eddies was minor, indicating a stronger uptake by diatoms in mature eddy. Nutrient concentrations at the depth of 150–300 m, on the other hand, showed similar levels among three water types. The ratios of N+N, SRP and Si(OH)₄ in both mature and decay eddies were all close to 1 relative to non-eddy waters.

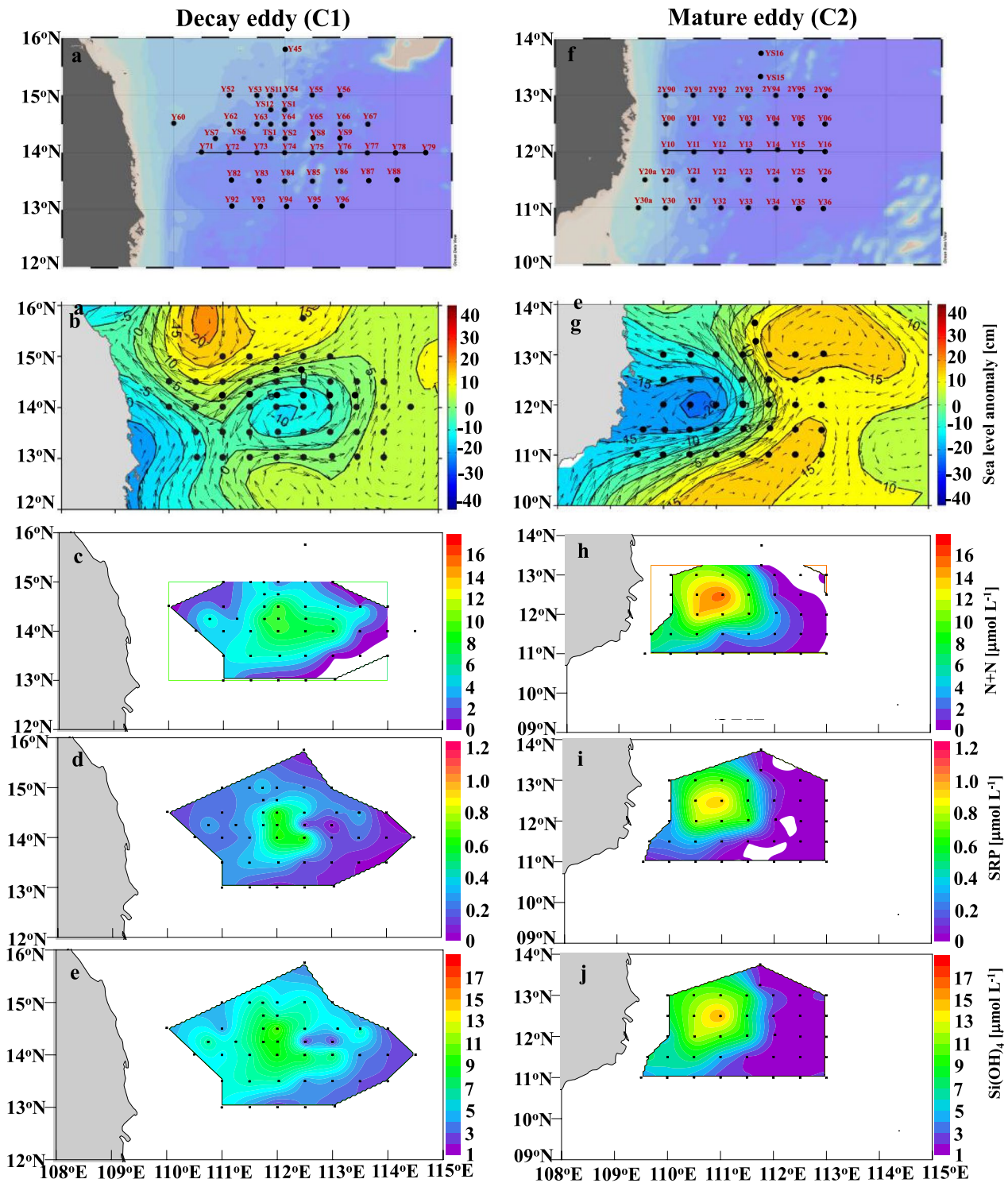


Fig. 1 Sampling maps for decay eddy (C1, **a**) and mature eddy (C2, **f**). Also shown are surface distributions of sea level anomalies (SLA) on 20 August **b** for decay eddy and 5 September, 2007 **g** for mature eddy. Sampling stations for nutrients (black dots) were also superimposed. Surface distributions of N + N, SRP and Si(OH)₄ at the depth of 50 m in decay eddy (**c**, **d**, **e**) and mature eddy (**h**, **i**, **j**). The chosen transects are highlighted in the sampling maps as black lines

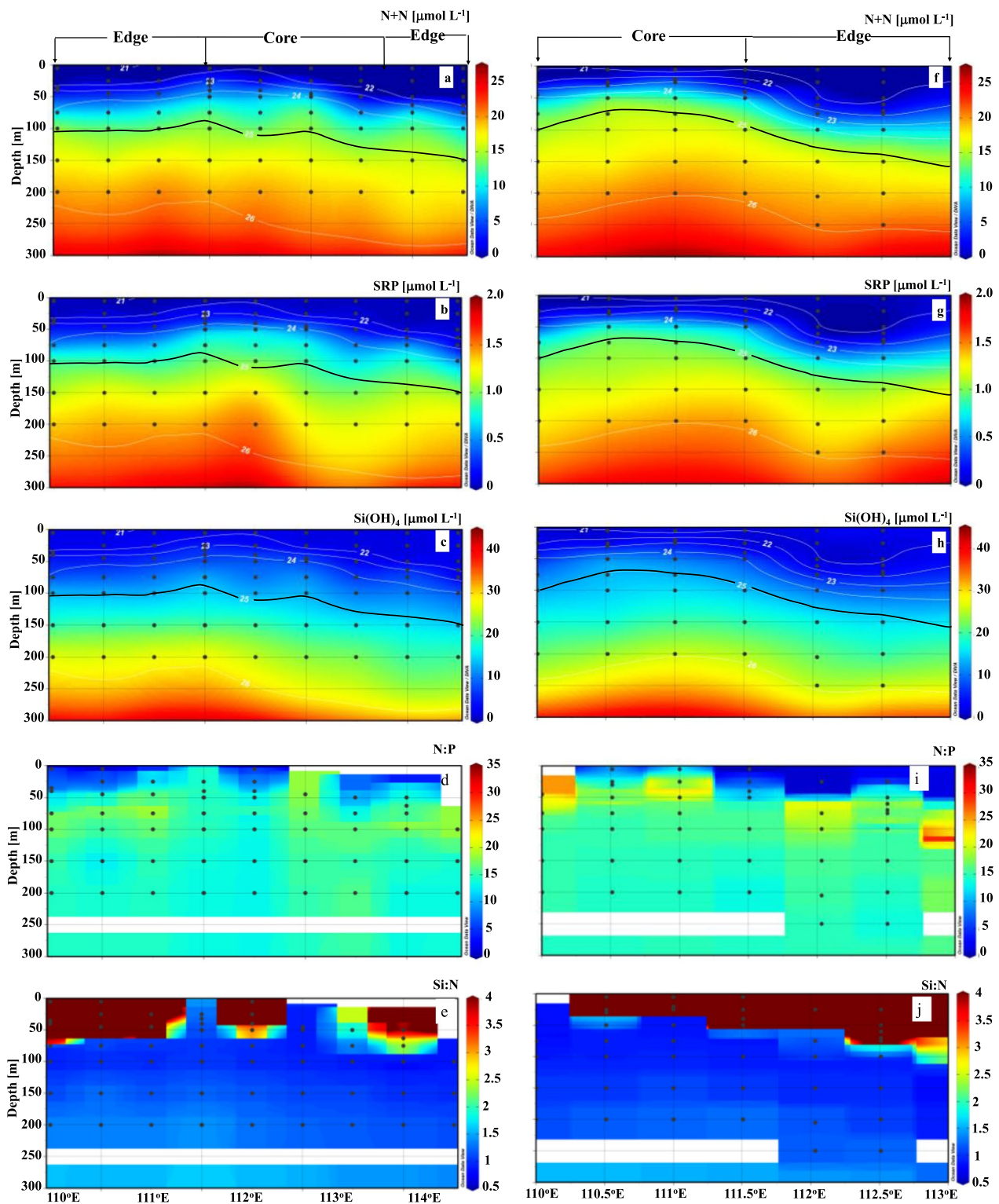


Fig. 2 Sectional distributions of N + N, SRP, Si(OH)_4 , dissolved N:P and Si:N ratios in the upper 300 m in decay eddy (left panel) and mature eddy (right panel) (see Fig. 1 for the locations of the transects). Core and edge stations are denoted at the top. The isopycnal lines of $\sigma_\theta = 25$ are also highlighted in black

Table 1 Nutrient concentrations and ratios (mean \pm standard deviation) in both dissolved and particulate phases, and biomass and phytoplankton community composition in three water types: eddy C2 (mature stage), eddy C1 (decay stage) and non-eddy water (SouthEast Asian Time-series Study (116°E, 18°N))

Parameter	C2(mature)	C1(decay)	Non-eddy
^a Age (d)	15–20	47–57	–
^b N + N (0–100 m, $\mu\text{mol L}^{-1}$)	6.6 \pm 3.7	5.0 \pm 1.7	1.7 \pm 0.84
^b SRP (0–100 m, $\mu\text{mol L}^{-1}$)	0.44 \pm 0.02	0.35 \pm 0.12	0.13 \pm 0.06
^b Si(OH) ₄ (0–100 m, $\mu\text{mol L}^{-1}$)	7.5 \pm 2.7	6.6 \pm 1.6	3.6 \pm 0.64
^b N + N (150–300 m, $\mu\text{mol L}^{-1}$)	20 \pm 1.7	20 \pm 1.2	18 \pm 2.3
^b SRP (150–300 m, $\mu\text{mol L}^{-1}$)	1.4 \pm 0.1	1.4 \pm 0.1	1.3 \pm 0.18
^b Si(OH) ₄ (150–300 m, $\mu\text{mol L}^{-1}$)	27 \pm 2.8	28 \pm 2.3	25 \pm 4.0
^c N/P @ SCM	21.2 \pm 7.5	15.0 \pm 4.3	13.2 \pm 7.0
N/P (0–100 m)	19.1 \pm 6.9	14.3 \pm 3.9	14.7 \pm 5.9
N/P (150–300 m)	15.0 \pm 0.76	13.8 \pm 0.86	14.5 \pm 1.2
^c Si/N @SCM	1.3 \pm 0.64	1.7 \pm 0.93	3.2 \pm 2.3
Si/N (0–100 m)	1.1 \pm 0.55	1.8 \pm 2.3	1.9 \pm 1.8
Si/N (150–300 m)	1.3 \pm 0.19	1.4 \pm 0.19	1.2 \pm 0.28
^b SiO ₂ (0–100 m, mmol m^{-2})	33 \pm 9	12 \pm 4	9
PN (0–100 m, mmol m^{-2})	37 \pm 5	30 \pm 4	24
bSiO ₂ /PN (0–100 m)	1.4 \pm 1.1	0.5 \pm 0.33	0.4 \pm 0.16
bSiO ₂ /POC (0–100 m)	0.16 \pm 0.018	0.082 \pm 0.069	0.06 \pm 0.027
^d $\Delta\text{N}/\Delta\text{P}$	10–16	10–16	–
^d $\Delta\text{Si}/\Delta\text{N}$	1–2	1–2	–
^b TChl <i>a</i> (0–100, mg m^{-2})	25.3 \pm 7.3	22.7 \pm 5.8	13 \pm 4.1
^b Fucoxanthin (0–100 m, mg m^{-2})	2.1 \pm 1.1	1.7 \pm 0.8	0.6 \pm 0.2
^b Diatom abundance (0–100 m, 10^7 cells m^{-2})	2.1 \pm 0.9	0.8 \pm 0.2	–
^e Diatom biomass percent (%)	7.6 \pm 6.6	2.2 \pm 2.0	–
Diazotroph abundance (0–100 m, 10^3 cell m^{-2})	1.2 \pm 1.0	1.0 \pm 0.3	–
^f Nutrient intrusion flux@150 m ($\text{mmol N m}^{-2} \text{d}^{-1}$)	70 \pm 4	11 \pm 1	–
^b Primary Production (0–100 m, $\text{mmol N m}^{-2} \text{d}^{-1}$)	11.2	10.7	1.9

SRP soluble reactive phosphorus, bSiO₂ biogenic silica

^a The age of the eddies is estimated based on the evolution of sea level anomalies, and the non-eddy water is considered as the initial timepoint of the eddies;

^b Values are mean \pm standard deviation of the averages of the depth integrated concentrations;

^c SCM: subsurface Chlorophyll Maximum;

^d $\Delta\text{N}/\Delta\text{P}$ and $\Delta\text{Si}/\Delta\text{N}$ represent the diatom nutrient uptake ratios simulated by a 1-D inverse model;

^e The diatom biomass percent (relative to total biomass) was estimated by acquiring the relative contribution of taxa (individual pigment) to the total chlorophyll *a* using the chemical taxonomy program, CHEMTAX (Wang et al. 2016)

^f Nutrient intrusion fluxes are first order estimates obtained by multiplication of the upwelling rate and the average nitrate + nitrite (N + N) concentration at 150 m, where biological assimilation was negligible

N/P and Si/N in dissolved and particulate form in two eddies

The dissolved N/P and Si/N nutrient ratios in three water types (i.e., non-eddy, mature eddy and decay eddy) showed similar vertical patterns with variable values, exhibiting a wider range in the upper 100 m but relatively stable below 100 m (Fig. 2). In the upper 100 m, both N/P < 16 and > 16 co-existed in three water types (Fig. 3a, e, i). The high N/P of > 16 was usually observed in the eddy center, where the upward water displacement was most significant, while low N/P was mostly seen at edges. Noted that ammonia was not included for N/P

ratio calculation. Zhu et al. (2021) reported an ammonia concentration range of 10–20 nmol L^{-1} in the SCS basin, which was overall < 5% of total dissolved N, and was thus excluded in the calculation of N/P ratios.

It is noteworthy that N/P ratios in the upper 100 m was ~1.4-fold higher in mature eddy relative to the other two water types ($P < 0.05$). The mean N/P ratio of 0–100 m for mature eddy was up to 19.1, which is higher than that observed in subsurface water (~14) and the Redfield ratio of 16. Likewise, the Si/N ratios in the upper 100 m for the three water types were also quite variable, being 0.9–3.1 (mature eddy), 0.8–18.3 (decay eddy) and

0.9–6.0 (non-eddy), comparing with values of 1.0–1.6, 1.1–1.6, 1.1–2.1 and 1.0–1.8, respectively, for 150 to 300 m depth interval. The mean Si/N ratio for upper 100 m in decay eddy (1.1 ± 0.55 as shown in Table 1) was lower than those (1.8–1.9) in the other two water types with 90% confidence interval ($P=0.07$). Overall, most of those high N/P ratios were observed near the SCM layers regardless the water type and the mature stage hold the highest N/P when the N+N concentration was lower than $10 \mu\text{mol L}^{-1}$ (Fig. 3b). Similarly, high dissolved Si/N values appeared near the SCM relative to the subsurface water (150–300 m) regardless water type, while the mature stage held lower Si/N values in the upper water column among three water types.

As for the particulate phase, significantly higher bSiO_2/PN appeared at the mature stage. For instance, the bSiO_2/PN ratios in the upper 100 m was 2.8-fold and 3.5-fold higher compared to those in decay eddy and non-eddy reference, respectively (Table 1 and Fig. 3). The enhancement of bSiO_2/PN in mature eddy is consistent with the growth of diatoms. The concentration of Fucoxanthin (average = $16.1 \pm 22.4 \text{ ng L}^{-1}$) in the upper 150 m of mature eddy was 1.5-fold and 3.0-fold higher than the values in the decay eddy (average = $10.6 \pm 10.6 \text{ ng L}^{-1}$) and non-eddy references (average = $5.4 \pm 5.0 \text{ ng L}^{-1}$).

Model-derived N/P and Si/N

In the model, the depth profiles of dissolved N/P for both mature and decay eddies have been simulated under different scenarios of the uptake ratio by diatoms. If the uptake ratio was set as 16 (Redfield ratio), the dissolved N/P in the upper 100 m would be less than 16 for both eddies (orange lines in Fig. 4). Once the uptake ratio was reduced to 10, the dissolved N/P presented elevated values of >16 in the SCM layer, where most of the diatom resided (blue lines in Fig. 4). Such increase of N/P is more obvious in mature eddy compared to decay eddy. For example, N/P reached to ~ 35 in mature eddy, while it was <25 in decay eddy. The depth profiles of dissolved Si/N are also presented in Fig. 4. Similar with N/P, Si/N also showed higher values (>1) in the SCM layer when Si/N uptake ratio by diatoms is assumed to be 1–2. Possibly due to the faster Si(OH)_4 uptake by diatoms, such Si/N elevation in the subsurface is less obvious in the mature eddy.

Discussion

In our case, the dissolved N/P ratios of subsurface nutrient source (below 150 m) were 14–15, lower than the classical Redfield ratio. Under the scenario of Redfield uptake, the N/P ratios of remaining nutrient in the euphotic zone should be less than the Redfield ratio. The consecutive changes in dissolved N/P ratio and its elevation during the mature stage of eddy in this study might thus be caused by several reasons: (1) preferential utilization of P relative to N; (2) N addition through N_2 -fixation and/or N deposition; (3) preferential P loss relative to N by particle sinking and/or active migration; and/or (4) stronger N than P supply from the remineralization of dissolved organic matter (DOM).

The phytoplankton community has been investigated for both eddies (Wang et al. 2016; Zhou et al. 2020). The abundance of diatom determined by microscope in upper 100 m was almost doubled in the mature eddy than the decay eddy (Table 1). Based on pigment analysis, Wang et al. (2016) showed that the diatom biomass in the upper 100 m in mature eddy was 21 times higher than that in non-eddy references, while other phytoplankton groups (e.g., Prasinophytes and Dinoflagellates) only showed 1.7–1.8-fold increase in pigment, demonstrating that diatom was the most enhanced groups. The increase in diatom abundance in mature eddy relative to decay eddy was consistent with \sim three-fold enhancement of bSiO_2 inventories concentrations at 0–100 m ($33 \text{ vs. } 12 \text{ mmol Si m}^{-2}$).

The increase in the dissolved N/P ratio (to 19.1 ± 6.9) in the upper ocean especially at the SCM layer during the mature stage might thus be largely related to the preferential P uptake by the diatom community (mainly comprised of *Thalassionema nitzschioides*, *Chaetoceros spp.*, and *Coscinodiscus spp.*, Zhou et al. (2020)). The contribution from other large cell species would be minor due to their low percentage in total biomass (Wang et al. 2016). The elevation of N/P ratio by the diatom utilization was further verified by our model practice. It has indicated that the diatom uptake ratio should be modulated by an N/P ratio of ~ 10 and Si/N of 1–2 to allow realistic simulation of the dissolved N/P and Si/N profiles with the best fit to observations (Fig. 4). The model-derived nutrient uptake ratio by

(See figure on next page.)

Fig. 3 Vertical profiles of N/P ratios (a, e, i), N/P ratios vs. N+N concentrations (b, f, j), bSiO_2/PN (c, g, k) and the diatom pigment fucoxanthin (d, h, l), in three different water types: non-eddy water (blue color), mature eddy (green color) and decay eddy (red color). The lines of $\text{N/P} = 16$ and $\text{Si/N} = 1$ are also shown as black solid lines. The dashed black lines are the average lines for those $\text{N/P} < 16$ and $\text{N/P} > 16$. The profiles of fluorescence were also shown with N/P ratios and diatom pigment. Note that the fluorescence scale for mature eddy is set differently from decay eddy and non-eddy water. For c, g and k, the left and right whisker represent the 10th and 90th percentile of bSiO_2/PN data from the same depth of all stations, respectively. The left and right boundaries of the box represent 25th and 75th data percentiles, respectively, with the central line representing the data median

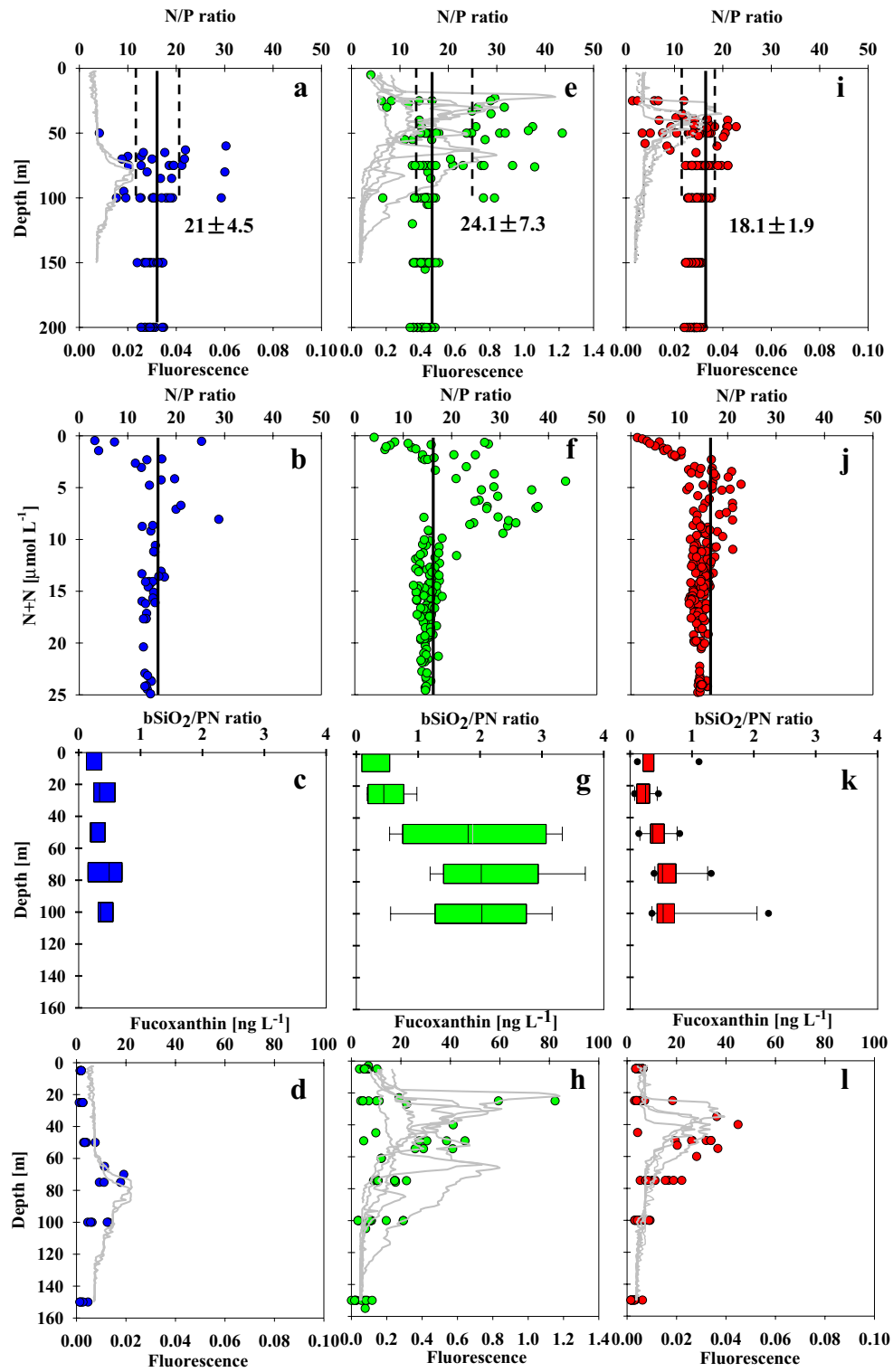


Fig. 3 (See legend on previous page.)

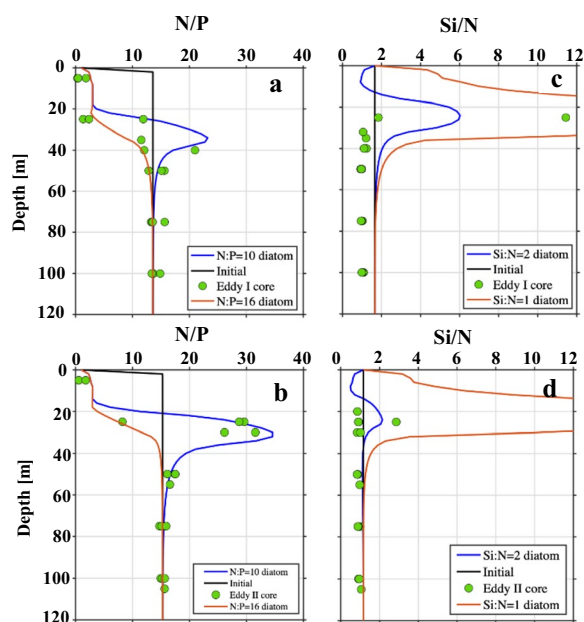


Fig. 4 Model-derived vertical N/P ratios (a, b) and Si/N ratios (c, d) in decay eddy and mature eddy by assuming a diatom uptake N/P ratio of 16 (orange line) and 10 (blue line) and Si/N ratio of 2 (blue line) and 1 (green line), respectively. Here, the uptake N/P ratios for non-diatoms are arbitrarily set as 16. The green dots are the in situ N/P and Si/N ratios in both C1 and C2 cores; the black line shows the N/P and Si/N profiles controlled only by physical upwelling and mixing

diatoms agreed well with cellular N/P ratio of the diatoms (Quigg et al. 2003; Weber and Deutsch 2010).

The Si/N ratios were also elevated in the upper ocean relative to the depth of 150 m. Under the higher growth rate or in high nutrient condition, the measured uptake ratio for diatoms could be > 1 (Hutchins & Bruland 1998; Brzezinski 1985). Indeed, the dissolved Si/N ratios in the upper depth of 0–100 m was significantly lower in mature eddy, which accounts for 60% of those in the decay eddy and non-eddy water. In addition, the reduction in Si/N in the dissolved phase in the mature eddy compared to the other two water types (i.e., decay eddy and non-eddy) also corresponded consistently to the elevation of $bSiO_2/PN$ (also $bSiO_2/POC$ shown in Table 1) in the particulate phase, i.e., 1.4 vs. 0.4–0.5 (mol:mol).

On the other hand, preferential P loss relative to N by particle sinking or active zooplankton migration is likely not a dominant driver for the elevated dissolved N/P ratios. It has been observed that P could be remineralized faster in marine particles compared to N (e.g., Schneider et al., 2003). Meanwhile, the stronger N supply (than P) by DOM remineralization is possible due to the higher N/P ratio of 19–22 measured in DOM (e.g., Hung et al. 2003), but these N/P ratios are still lower than

those from the mature eddy. In addition, as the regional closeness between the two eddies, it seemed impossible to induce such obvious difference of N/P ratios by DOM remineralization. Finally, the elevated N/P ratios during the eddy evolution was unlikely induced by the N-addition through N_2 -fixation or its associated enhancement of P consumption, and/or N-deposition in our study. The N_2 -fixation rate has been measured in various parts of the SCS (Lu et al. 2019; Voss et al. 2006; Zhang et al. 2015) showing low N_2 -fixation rates and accounting for only a very small fraction ($< 5\%$) of the primary production (PP) in the SCS (Lu et al. 2019; Voss et al. 2006). The N_2 -fixation rate was not measured in current study; however, the abundance of diazotrophs (e.g., *Trichodesmium* and *Richelia*) was comparable between eddies (Table 1). If the abundance was converted into the N_2 -fixation rate (Bonnet et al. 2018), the values could be as low as $< 1.0 \mu\text{mol N m}^{-2}\text{d}^{-1}$ which was even less than the reported N_2 -fixation rate in the northern SCS (Lu et al. 2019). Indeed, nitrogen fixers are not dominant, where nutrient rich waters are upwelled like mesoscale eddies. In addition, first order estimates of the nutrient intrusion flux by eddy pumping might be sufficient to support the PP determined in the eddies (Table 1). It can thus be concluded that N_2 -fixation may play only a minor role in explaining the N/P elevation during the eddy's mature phase. More importantly, our results are consistent with the concept proposed by Mills and Arrigo (2010) that the enhanced subsurface diatom growth by eddy pumping may filter P preferentially to hamper the P supply, thus, the niche development of N_2 -fixers in surface water. On the other hand, the N deposition was equally important relative to N_2 -fixation in the SCS (Yang et al. 2014). In the present study, however, its contribution to the elevated N/P ratio could be excluded, since both decay and mature eddy were located in the same region receiving similar N deposition.

We noted that low N/P ratios ($< 16:1$) occurred above the SCM for both eddies, which could be a result of a high N/P uptake ratio by other phytoplankton taxa such as *Prochlorococcus* and *Synechococcus* (Singh et al. 2017) as well as preferential release of P relative to N by particle remineralization (Clark et al. 1998; Monteiro and Follows 2012). The preferential release of P could be the case particularly in decay eddy, where shallow remineralization was observed as indicated by excess ^{234}Th (Zhou et al. 2020).

As mesoscale eddies are ubiquitous physical features in the ocean, the non-Redfield N/P ratio and its temporal evolution resulting from the growth and recession of diatom within eddies may be of great significance to nutrient dynamics, especially the modulation of N_2 -fixation at the surface (Fig. 5). During the mature stage with eddy

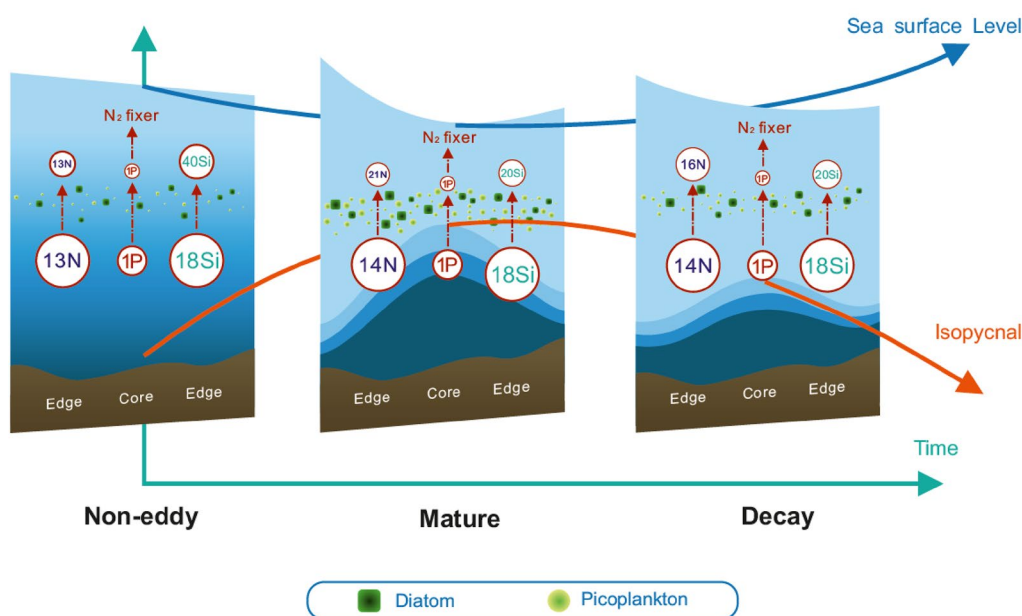


Fig. 5 Conceptual model of nutrient dynamics within eddies at different developmental stages in the cyclonic eddies of western South China Sea modified from Zhou et al. (2020). The size of the circles denotes the relative nutrient concentration; nutrient ratios are shown in the circles

pumping, P was preferentially assimilated in the SCM layer resulting in elevated N/P ratios (> 16:1) in remaining water in the upper layer (especially SCM layer). At this stage, the niche development of N₂-fixers was modulated by subsurface diatom growth. During the decay stage, although P assimilation rate decreased due to the decline in diatom abundance, the vertical P supply was also reduced due to eddy recession. This scenario suggests a synergistic impact of coupled physical–biological processes on vertical niche modulation, which could improve our understanding of phytoplankton competition in vertical scale and potentially benefit the parameterization of current biogeochemical models (Mills and Arrigo 2010). To examine the temporal evolution of nutrient dynamics, the ideal strategy is to observe on single eddy over its entire lifespan. However, it is extremely difficult for shipboard measurements that include nutrient concentrations and dynamics due to the need of temporally and spatially resolved sampling. This study happened to encounter two eddies at different evolution stages that could mimic the eddy evolution as an alternatively best approach. Moreover, the two eddies were formed in the similar region by the same physical forcing of the coastal jet separation and are believed to experience the similar temporal evolution (Zhou et al. 2020).

However, the high dissolved N/P ratios had not been reported in the SCS basin and North Pacific Subtropical gyre in previous studies (Du et al. 2013; Wong et al. 2007; Deutsch and Weber 2012) indicating that such an

eddy-induced high N/P ratio phenomenon was transient and was likely missed by routine field observations. Our results further emphasize that cautions should be made using subsurface nutrient ratios to derive N* (= N-16P) for N₂-fixation estimate in oligotrophic oceans (Deutsch et al. 2001; Hansell et al. 2004; Singh et al. 2013; Wong et al. 2007).

Conclusions

Nutrient ratios were measured to be higher than the canonical Redfield ratio in a mature cyclonic eddy in the western SCS, while they were lower than Redfield ratio in another eddy under the decay stage. We found that such variability in the nutrient ratios within eddies is tightly linked to the temporal evolution in the abundance and nutrient uptake of large-cell diatoms, mediated by the physical dynamics of eddies. It implies that the regional nutrient addition by N₂-fixation could be overestimated if such a high N/P ratio was used as a tracer for N₂-fixation rate. The time series of nutrient ratios needs to be fully investigated in the eddies to understand the nutrient dynamics in the ocean.

Abbreviations

N/P	Nitrate + nitrite to soluble reactive phosphorus
CE	Cyclonic eddy
SCS	South China Sea
POC	Particulate organic carbon
PN	Particulate nitrogen
bSiO ₂	Biogenic silica

CTD	Conductivity–temperature–depth
SRP	Soluble reactive phosphorus
CoSiNE	Carbon, Silicate, Nitrogen Ecosystem
SLA	Sea Level Anomaly
SCM	Subsurface Chl <i>a</i> maximum
BATS	Bermuda Atlantic time-series study
DOM	Dissolve organic matter
PP	Primary production

Supplementary Information

The online version contains supplementary material available at <https://doi.org/10.1186/s40562-023-00269-8>.

Additional file 1. The supplemental text S1: Verification of the model.

Acknowledgements

We thank the crew of R/V Dongfanghong II for much help during the sampling cruise, Hua Lin, Jian Ma, Xiao Huang, Aiqian Han and Min Zhang for helping with sampling and analysis. We also thank Drs. Jiwei Tian, Jianyu Hu and Jianping Gan for their suggestions during discussions. This study was supported by the National Natural Scientific Foundation of China through grants #41730533, #41890804 and #42188102.

Author contributions

All authors read and approved the final manuscript.

Availability of data and materials

The data set generated in this study are available in the Science Data Bank (<https://www.scidb.cn/en>).

Declarations

Competing interests

The authors declare that they have no competing interests.

Received: 3 November 2022 Accepted: 20 February 2023

Published online: 06 March 2023

References

- Arrigo KR, Robinson DH, Worthen DL, Dunbar RB, DiTullio GR, VanWoert M, Lizotte MP (1999) Phytoplankton community structure and the draw-down of nutrients and CO₂ in the Southern Ocean. *Science* 283:365–367
- Benitez-Nelson CR, McGillicuddy DJ (2008) Mesoscale physical–biological–biogeochemical linkages in the open ocean: an introduction to the results of the E-Flux and EDDIES programs. *Deep Sea Res Pt II* 55:1133–1138. <https://doi.org/10.1016/j.dsr.1132.2008.1103.1001>
- Benitez-Nelson CR, Bidigare RR, Dickey TD, Landry MR, Leonard CL, Brown SL, Nencioli F, Rii YM, Maiti K, Becker JW, Bibby TS, Black W, Cai WJ, Carlson CA, Chen F, Kuwahara VS, Mahaffey C, McAndrew PM, Quay PD, Rappé MS, Selph KE, Simmons MP, Yang EJ (2007) Mesoscale eddies drive increased silica export in the subtropical Pacific Ocean. *Science* 316:1017–1021. <https://doi.org/10.1126/science.1136221>
- Bonnet S, Caffin M, Berthelot H, Grosso O, Benavides M, Helias-Nunige S, Guiu C, Stenegren M, Foster RA (2018) In-depth characterization of diazotroph activity across the western tropical South Pacific hotspot of N₂ fixation (OUTPACE cruise). *Biogeosciences* 15:4215–4232
- Bruland KW, Rue EL, Smith GJ, DiTullio GR (2005) Iron, macronutrients and diatom blooms in the Peru upwelling regime: brown and blue waters of peru. *Mar Chem* 93:81–103
- Brzezinski MA (1985) The Si:C: N ratio of marine diatoms: interspecific variability and the effect of some environmental variables. *J Phycol* 21:347–357. <https://doi.org/10.1111/j.0022-3646.1985.00347.x>
- Clark LL, Ingall ED, Benner R (1998) Marine phosphorus is selectively remineralized. *Nature* 393:426–426. <https://doi.org/10.1038/30881>
- De Baar HJW, Van Leeuwe MA, Scharek R, Goeyens L, Bakker KMJ, Fritsche P (1997) Nutrient anomalies in *Fragilariopsis kerguelensis* blooms, iron deficiency and the nitrate/phosphate ratio (A. C. redfield) of the Antarctic Ocean. *Deep-Sea Res Pt II* 44:229–260
- Deutsch C, Weber T (2012) Nutrient ratios as a tracer and driver of ocean biogeochemistry. *Ann Rev Mar Sci* 4:113–141. <https://doi.org/10.1146/annurev-marine-120709-142821>
- Deutsch C, Gruber N, Key RM, Sarmiento JL, Ganachaud A (2001) Denitrification and N₂ fixation in the Pacific Ocean. *Global Biogeochem Cycles* 15:483–506
- DeVries T (2018) New directions for ocean nutrients. *Nat Geosci* 11:15–16. <https://doi.org/10.1038/s41561-41017-40042-z>
- Du C, Liu Z, Dai M, Kao SJ, Cao Z, Zhang Y, Huang T, Wang L, Li Y (2013) Impact of the Kuroshio intrusion on the nutrient inventory in the upper northern South China Sea: insights from an isopycnal mixing model. *Biogeosciences* 10:6419–6432
- Falkowski PG (2000) Rationalizing elemental ratios in unicellular algae. *J Phycol* 36:3–6. <https://doi.org/10.1046/j.1529-8817.2000.99161.x>
- Hansell DA, Bates NR, Olson DB (2004) Excess nitrate and nitrogen fixation in the North Atlantic Ocean. *Mar Chem* 84:243–265
- Hu J, Gan J, Sun Z, Zhu J, Dai M (2011) Observed three-dimensional structure of a cold eddy in the southwestern South China Sea. *J Geophys Res Oceans*. <https://doi.org/10.1029/2010JC006810>
- Hung J-J, Chen C-H, Gong G-C, Sheu D-D, Shiah F-K (2003) Distributions, stoichiometric patterns and cross-shelf exports of dissolved organic matter in the East China Sea. *Deep Sea Res Pt II* 50:1127–1145. [https://doi.org/10.1016/S0967-0645\(03\)00014-6](https://doi.org/10.1016/S0967-0645(03)00014-6)
- Hutchins DA, Bruland KW (1998) Iron-limited diatom growth and Si: N uptake ratios in a coastal upwelling regime. *Nature* 393:561–564
- Klausmeier CA, Litchman E, Daufresne T, Levin SA (2004) Optimal nitrogen-to-phosphorus stoichiometry of phytoplankton. *Nature* 429:171–174. <https://doi.org/10.1038/nature02454>
- Li QP, Hansell DA (2008) Nutrient distributions in baroclinic eddies of the oligotrophic North Atlantic and inferred impacts on biology. *Deep-Sea Res Pt II* 55:1291–1299
- Lu Y, Wen Z, Shi D, Lin W, Bonnet S, Dai M, Kao S-J (2019) Biogeography of N₂ fixation influenced by the western boundary current intrusion in the south china sea. *J Geophys Res-Oceans* 124:6983–6996
- Ma J, Yuan D, Liang Y (2008) Sequential injection analysis of nanomolar soluble reactive phosphorus in seawater with HLB solid phase extraction. *Mar Chem* 111:151–159
- Ma W, Xiu P, Chai F, Li H (2019) Seasonal variability of the carbon export in the central South China Sea. *Ocean Dynam* 69:955–966
- Martiny AC, Pham CTA, Primeau FW, Vrugt JA, Moore JK, Levin SA, Lomas MW (2013) Strong latitudinal patterns in the elemental ratios of marine plankton and organic matter. *Nat Geosci* 6:279–283
- McGillicuddy DJ Jr (2016) Mechanisms of physical-biological-biogeochemical interaction at the oceanic mesoscale. *Ann Rev Mar Sci* 8:125–159
- McGillicuddy DJ, Robinson AR, Siegel DA, Jannasch HW, Johnson R, Dickey T, McNeil J, Michaels AF, Knap AH (1998) Influence of mesoscale eddies on new production in the Sargasso Sea. *Nature* 394:263–266
- Mills MM, Arrigo KR (2010) Magnitude of oceanic nitrogen fixation influenced by the nutrient uptake ratio of phytoplankton. *Nat Geosci* 3:412–416
- Monteiro FM, Follows MJ (2012) On nitrogen fixation and preferential remineralization of phosphorus. *Geophys Res Lett*. <https://doi.org/10.1029/2012GL050897>
- Pai S-C, Yang C-C, Riley JP (1990a) Effects of acidity and molybdate concentration on the kinetics of the formation of the phosphoantimonymolybdenum blue complex. *Anal Chim Acta* 229:115–120
- Pai S-C, Yang C-C, Riley JP (1990b) Formation kinetics of the pink azo dye in the determination of nitrite in natural waters. *Anal Chim Acta* 232:345–349
- Quigg A, Finkel ZV, Irwin AJ, Rosenthal Y, Ho T-Y, Reinfelder JR, Schofield O, Morel FMM, Falkowski PG (2003) The evolutionary inheritance of elemental stoichiometry in marine phytoplankton. *Nature* 425:291–294
- Redfield AC (1958) The biological control of chemical factors in the environment. *Am Sci* 46:205–221
- Rii YM, Brown SL, Nencioli F, Kuwahara V, Dickey T, Karl DM, Bidigare RR (2008) The transient oasis: Nutrient-phytoplankton dynamics and particle export in Hawaiian lee cyclones. *Deep-Sea Res Pt II* 55:1275–1290

- Schneider B, Schlitzer R, Fischer G, Nothig E-M (2003) Depth-dependent elemental compositions of particulate organic matter (POM) in the ocean. *Global Biogeochem Cy* 17:1032. <https://doi.org/10.1029/2002GB001871>
- Singh A, Lomas MW, Bates NR (2013) Revisiting N₂ fixation in the North Atlantic Ocean: significance of deviations from the redfield ratio, atmospheric deposition and climate variability. *Deep-Sea Res Pt II* 93:148–158
- Singh A, Bach LT, Fischer T, Hauss H, Kiko R, Paul AJ, Stange P, Vandromme P, Riebesell U (2017) Niche construction by non-diazotrophs for N₂ fixers in the eastern tropical North Atlantic Ocean. *Geophys Res Lett* 44:6904–6913
- Sweeney EN, McGillicuddy DJ, Buesseler KO (2003) Biogeochemical impacts due to mesoscale eddy activity in the sargasso sea as measured at the bermuda atlantic time-series study (BATS). *Deep-Sea Res Pt II* 50:3017–3039
- Voss M, Bombar D, Loick N, Dippner JW (2006) Riverine influence on nitrogen fixation in the upwelling region off Vietnam South China Sea. *Geophys Res Lett*. <https://doi.org/10.1029/2005GL025569>
- Wang L, Huang B, Chiang KP, Liu X, Chen B, Xie Y, Xu Y, Hu J, Dai M (2016) Physical-biological coupling in the western south china sea: the response of phytoplankton community to a mesoscale cyclonic eddy. *PLoS ONE* 11:0153735
- Weber TS, Deutsch C (2010) Ocean nutrient ratios governed by plankton biogeography. *Nature* 467:550–554
- Wong GTF, Tseng C-M, Wen L-S, Chung S-W (2007) Nutrient dynamics and N-anomaly at the SEATS station. *Deep-Sea Res Pt II* 54:1528–1545
- Xiu P, Chai F (2020) Eddies affect subsurface phytoplankton and oxygen distributions in the north pacific subtropical gyre. *Geophys Res Lett* 47:112
- Xu YP, Dai MH, Zhai WD, Yuan DX, Liu JW, Sun ZY, Lin H, Wu JY (2009) Short-term dynamics of nutrients influenced by upwelling in a small oligotrophic coastal ecosystem Gan Bay, in the Northwest Philippines. *Prog Nat Sci* 19:595–601. <https://doi.org/10.1016/j.pnsc.2008.10.005>
- Yang JYT, Hsu SC, Dai MH, Hsiao SSY, Kao SJ (2014) Isotopic composition of water-soluble nitrate in bulk atmospheric deposition at Dongsha Island: sources and implications of external N supply to the northern South China Sea. *Biogeosciences* 11:1833–1846
- Zhang R, Chen M, Yang Q, Lin Y, Mao H, Qiu Y, Tong J, Lv E, Yang Z, Yang W, Cao J (2015) Physical-biological coupling of N₂ fixation in the northwestern South China Sea coastal upwelling during summer. *Limnol Oceanogr* 60:1411–1425
- Zhou K, Dai M, Kao S-J, Wang L, Xiu P, Chai F, Tian J, Liu Y (2013) Apparent enhancement of ²³⁴Th-based particle export associated with anticyclonic eddies. *Earth Planetary Sc Lett* 381:198–209
- Zhou K, Dai M, Xiu P, Wang L, Hu J, Benitez-Nelson CR (2020) Transient enhancement and decoupling of carbon and opal export in cyclonic eddies. *J Geophys Res Oceans* 11:110
- Zhu Y, Liu J, Mulholland MR, Du C, Wang L, Widner B, Huang T, Yang Y, Dai MH (2021) Dynamics of ammonium biogeochemistry in an oligotrophic regime in the South China Sea. *Mar Chem*. <https://doi.org/10.1016/j.marchem.2021.104040>

Publisher's Note

Springer Nature remains neutral with regard to jurisdictional claims in published maps and institutional affiliations.

Submit your manuscript to a SpringerOpen[®] journal and benefit from:

- Convenient online submission
- Rigorous peer review
- Open access: articles freely available online
- High visibility within the field
- Retaining the copyright to your article

Submit your next manuscript at ► [springeropen.com](https://www.springeropen.com)
